Zentrum für Technomathematik

Fachbereich 3 – Mathematik und Informatik

Quenching simulation for the induction hardening process – Thermal and mechanical effects

J. Montalvo-Urquizo Q. Liu A. Schmidt

Report 13–02

Berichte aus der Technomathematik

Report 13–02 **May 2013**

Quenching simulation for the induction hardening process – Thermal and mechanical effects

J. Montalvo-Urquizo[a,*], Q. Liu[a], A. Schmidt[a]

[a] *Zentrum für Technomathematik, University of Bremen, Germany*

Abstract

We investigate the mathematical model for induction hardening of steel and present simulation results for the involved cooling process. The model accounts for the thermomechanical effects coupled with phase transitions that are caused by the enormous changes in temperature during the heat treatment. The mechanical part of the quenching model includes the transformation strain and transformation plasticity induced by the phase transitions (TRIP). The simulations have been performed by assuming a non-homogeneous pre-heated workpiece with an austenite profile generated via high-frequency inductive heating. The mathematical ingredients of the model are presented and the main simulation results are reported for the case of a gearing component made of steel 42CrMo4.

Key words: Heat treatment, surface hardening, phase transitions, Transformation induced plasticity, Quenching

1. Introduction

For many applications in industry the surface of steel components is particularly stressed. Therefore, there exists a growing demand of surface hardened products. Hardening is a metallurgical and metalworking process used to increase the hardness of the boundary layers of a workpiece made of steel. The first step for hardening is the heating of the components to a temperature at which the iron phase changes from the initial phase into austenite.

*Corresponding author

Email addresses: montalvo@math.uni-bremen.de (J. Montalvo-Urquizo), liu@math.uni-bremen.de (Q. Liu), schmidt@math.uni-bremen.de (A. Schmidt)

Then the material is quenched by applying high cooling rates on it. The reason why the hardness of steel can be changed relies on the occurring phase transitions. In the case of surface hardening, high cooling rates should be achieved so that most of the austenite phase is transformed to martensite by a diffusionless phase transition, producing the desired hardening effect.

Induction hardening is one of the most important surface hardening procedures and has been successfully applied in industry for more than 50 years. In this heat treatment method, an induction coil is connected to the power supply and the flow of alternating current through the coil generates an alternating magnetic field which in turn induces eddy currents in the workpiece. The energy dissipated due to these currents causes heat in the steel component and can be used to heat up only a specific part of it.

Although the inductive hardening is well established among practitioners, the needs for process optimization are still open. In this sense, the modeling, numerical simulation, and optimization remain areas of great interest in the applied research.

In this paper, we report on the research performed for a subproject of the network *MeFreSim–Modeling, Simulation and Optimization of Multi-Frequency Induction Hardening as Part of Modern Production* formed by the Weierstraß-Institut für Angewandte Analysis und Stochastik (Berlin), the Zentrum für Technomathematik (Universität Bremen), the Institut für Mathematik (Universität Augsburg), the Stiftung Institut für Werkstofftechnik (Bremen), and the industrial partners EFD Induction GmbH and ZF Friedrichshafen AG.

We present here our work performed within the research network, consisting of the numerical simulation of thermomechanical effects due to the phase transitions during the quenching process of gear components.

This work deals with the model and simulation for the quenching process after a high-temperature profile has been achieved with an inductor on a gearing component. The rather general model for quenching of steel is presented in Section 2, including heat conduction, phase transformations, thermoelasticity and transformation induced plasticity (TRIP) to be considered in the computations. After this, Section 3 presents the material data, simulation setting and main results for an implementation of a gearing component made of steel 42CrMo4. The final Section 4 draws some concluding remarks and present some ideas for further research.

2. The mathematical model

For the complete heat treatment cycle we usually consider four characteristic times: the beginning of the heating process t_0 (at room temperature), the end of the heating process t_1, the end of a mantained high temperature $\tilde{t}_1$, and the end of the quenching process t_2. In the case of induction hardening the stabilization period $[t_1, \tilde{t}_1]$ is very small and can be neglected such that the process is only characterized by the heating interval $[t_0, t_1)$ and the quenching interval $[t_1, t_2]$.

At time t_0 steel is assumed to consist of a mixture of ferrite, pearlite, bainite, and some martensite (the last one typically representing the smallest amount). Unfortunately the exact phase distribution of such mixture of phases is unknown in practice and represents an uncertainty factor in the model. For this reason we introduce the symbol Z^0 which will be reserved in the following for the initial phase mixture prior to the heat treatment. During the heating process Z^0 is (partially) transformed to austenite. Later, during the (rapid) cooling stage, the austenitic phase is transformed mainly into marteniste, but it may also be transformed into ferrite, pearlite, and bainte in a much smaller portion; the remaining volume fraction of Z^0 remains unchanged.

A good model for describing the heat treatment of steel is based on the thermal and mechanical equations for the description of temperature and mechanical deformations in the material pieces. Similar models with coupled equations for thermomechanical problems have been previously simulated for processes like heat treatment, welding and shape rolling, among others (cf. e.g. [1], [5], [12], [14]).

The rapid cooling rates are obtained by prescribing appropriate boundary conditions in a heat equation and the temperature gives rise to the time evolution of the single phases. The coupling between the thermal and the mechanical models is determined by the density changes in material resulting from temperature and phase changes, as well as by the mechanical dissipation. At the same time, the phases' evolution is a direct consequence of the temperature changes, as described below.

2.1. The phase transitions

Mathematical models for phase transitions in steel have been considered e.g. in [4]–[6], [8], [14], [17], [18], [19]. In many works, the description of the

diffusive phase transitions in the isothermal case is done via the Johnson-Mehl equation. In order to establish a general model for isothermal multi-phase case during the cooling process we introduce the following notations:

- $z^0(t)$: the volume fraction of Z^0, i.e., the mixture of phases present before the heating process,
- z_0^1: the volume fraction of austenite at time t_1 which stands for the end-time of the heating process (i.e. the start of quenching)
- $z^1(t)$: the volume fraction of remaining austenite during the cooling process, and,
- $z^2(t), \cdots, z^5(t)$: volume fraction of ferrite, pearlite, bainite, martensite, which have been transformed from austenite during cooling.

As mentioned, the workpiece has the phase configuration Z^0 at time t_0, thus we have $z^0(t_0) = 1$. Since the outer layers of the workpiece have been transformed to austenite from Z^0 during the heating process, it is observed that the phases at the end of heating correspond to a portion of Z^0 and a portion of austenite, it is $z^0(t_1) + z^1(t_1) = 1$.

During quenching, austenite is transformed into ferrite, pearlite, bainite and marteniste, then we can conclude

$$z^1(t_1) \equiv z_0^1 = z^1(t) + z^2(t) + z^3(t) + z^4(t) + z^5(t) \text{ for } t \in (t_1, t_2].$$

and the remaining fraction of Z^0 remains unchanged during cooling and equals to $z^0(t_1)$.

We describe the evolution of volume fractions during the cooling process which occurs for $t \in [t_1, t_2]$ by the following equations

$$\begin{cases} z^2(t) + z^3(t) &= z_0^1 \left(1 - e^{-b(\theta)(t-t_1)^{a(\theta)}}\right) & \text{for } F_{P_f} \le \theta \le F_{P_s}, \\ z^4(t) &= (z_0^1 - (z^2(t) + z^3(t))) \left(1 - e^{-\tilde{b}(\theta)(t-t_1)^{\tilde{a}(\theta)}}\right) & \text{for } B_f \le \theta \le B_s, \\ z^5(t) &= (z_0^1 - z^2(t) - z^3(t) - z^4(t)) \left(1 - \left(\frac{\theta - M_f}{M_s - M_f}\right)^n\right) & \text{for } M_f \le \theta \le M_s, \end{cases} \tag{1}$$

where the evolutions of ferrite, pearlite and bainite (the first and the second equations) arise from the Johnson-Mehl-Avrami equation and the austenite-marteniste phase change (the third equation) is from Schröder's approach,

see e.g. [13]. The parameters $b(\theta)$, $a(\theta)$, $\tilde{b}(\theta)$, $\tilde{a}(\theta)$ and n have to be identified using experimental data as in [11]. $F_{P_s}(F_{P_f})$, $B_s(B_f)$, and $M_s(M_f)$ denote the start (end) temperatures of formations of ferrite/pearlite, bainite and martensite, respectively.

The equations (1) may be then be reduced to a system of ODEs. For simplicity, let $\tilde{z}$ denote z^2+z^3, then it is easy to verify from the first equation in (1) that

$$t - t_1 = \left(\frac{\ln\left(1 - \dfrac{\tilde{z}}{z_0^1}\right)}{-b(\theta)} \right)^{1/a(\theta)} . \tag{2}$$

Formal differentiation of (2) with respect to time gives the ordinary differential equation

$$\dot{\tilde{z}} = -a(\theta)b(\theta)^{1/a(\theta)}(z_0^1 - \tilde{z}) \left(\ln\left(1 - \frac{\tilde{z}}{z_0^1}\right)\right)^{1-\frac{1}{a(\theta)}} . \tag{3}$$

In a similar manner, using the second equation in (1) one gets

$$\dot{z}^4 = -\tilde{a}(\theta)\tilde{b}(\theta)^{1/\tilde{a}(\theta)}(z_0^1 - \tilde{z} - z^4) \left(\ln\left(1 - \frac{z^4}{z_0^1 - \tilde{z}}\right)\right)^{1-\frac{1}{\tilde{a}(\theta)}} - \frac{z^4\dot{\tilde{z}}}{z_0^1 - \tilde{z}}. \tag{4}$$

and then the problem (1) is equivalent to the initial-value ODEs

$$\begin{cases} \dot{\tilde{z}} = -a(\theta)b(\theta)^{1/a(\theta)}(z_0^1 - \tilde{z}) \left(\ln\left(1 - \dfrac{\tilde{z}}{z_0^1}\right)\right)^{1-\frac{1}{a(\theta)}} \mathcal{H}(\theta - F_{P_f})\mathcal{H}(F_{P_s} - \theta), \\ \dot{z}^4 = \left(-\tilde{a}(\theta)\tilde{b}(\theta)^{1/\tilde{a}(\theta)}(z_0^1 - \tilde{z} - z^4) \left(\ln\left(1 - \dfrac{z^4}{z_0^1 - \tilde{z}}\right)\right)^{1-\frac{1}{\tilde{a}(\theta)}} - \dfrac{z^4\dot{\tilde{z}}}{z_0^1 - \tilde{z}} \right) \times \\ \qquad \times \mathcal{H}(\theta - B_f)\mathcal{H}(B_s - \theta), \\ \dot{z}^5 = \left(\dfrac{d}{dt}\left((z_0^1 - \tilde{z} - z^4)\left(1 - \left(\dfrac{\theta - M_f}{M_s - M_f}\right)^n\right)\right)\right) \mathcal{H}(\theta - M_f)\mathcal{H}(M_s - \theta), \\ \tilde{z}(t_1) = z^4(t_1) = z^5(t_1) = 0, \end{cases} \tag{5}$$

where $\mathcal{H}$ denotes the heaviside step function.

2.2. Thermomechanical modeling

We assume small deformations and consider the balance law of momentum without inertial term together with the balance of internal energy as

$$\begin{aligned} -\operatorname{div}\sigma &= 0, \qquad (6)\\ \varrho\dot{e} + \operatorname{div} q &= \sigma : \varepsilon(\dot{u}) + h, \qquad (7) \end{aligned}$$

which are essential to determine the displacement u, the stress tensor σ and the temperature θ. Here ϱ is the mass density, q is the heat flux, e the specific internal energy, $\varepsilon(\dot{u}) = \frac{1}{2}(\nabla\dot{u} + \nabla\dot{u}^T)$ the symmetric part of the strain rate tensor and h the external heat source. Further, we assume that the total strain $\varepsilon(u)$ can be additively decomposed in an elastic part $\varepsilon^{\mathrm{el}}$, a thermal part $\varepsilon^{\mathrm{th}}$, and a TRIP part $\varepsilon^{\mathrm{trip}}$ (cf. [7] for details), i.e.

$$\varepsilon(u) = \varepsilon^{\mathrm{el}} + \varepsilon^{\mathrm{th}} + \varepsilon^{\mathrm{trip}}. \qquad (8)$$

We describe the thermal strain as the thermal expansion produced by density changes, it is

$$\varepsilon^{\mathrm{th}} = \left(\left(\frac{\varrho^0(\theta_{ref})}{\varrho(\theta, z)} \right)^{\frac{1}{3}} - 1 \right) I.$$

where $\varrho^0(\theta_{ref})$ stands for the homogenous measured density of the initial phase configuration $z^0(t_0)$ at reference temperature θ_{ref} and we make a mixture ansatz for the density as

$$\varrho(\theta, z) = \sum_{i=0}^{5} z^i \varrho^i(\theta), \qquad (9)$$

where $\varrho^i(\theta)$ is the homogenous temperature-dependent density of the phase z^i at temperature θ. Moreover the thermal part $\varepsilon^{\mathrm{th}}$ can be subsequently decomposed in an isothermal phase transition effect at reference temperature θ_{ref} and a thermal expansive part without phase transitions, i.e.

$$\begin{aligned} \varepsilon^{\mathrm{th}} &\approx \left(\left(\frac{\varrho^0(\theta_{ref})}{\varrho(\theta_{ref}, z)} \right)^{\frac{1}{3}} - 1 \right) I + \sum_{i=0}^{5} z^i \alpha^i(\theta)(\theta - \theta_{ref}) I \\ &\approx -\frac{1}{3} \left(\frac{\varrho(\theta_{ref}, z)}{\varrho^0(\theta_{ref})} - 1 \right) I + \sum_{i=0}^{5} z^i \alpha^i(\theta)(\theta - \theta_{ref}) I \qquad (10)\\ &= -\frac{1}{3} \sum_{i=0}^{5} z^i \left(\frac{\varrho^i(\theta_{ref})}{\varrho^0(\theta_{ref})} - 1 \right) I + \sum_{i=0}^{5} z^i \alpha^i(\theta)(\theta - \theta_{ref}) I, \end{aligned}$$

here $\alpha^i(\theta)$ is the linear thermal expansion coefficient of the phase z^i where we assume the density $\varrho^i(\theta)$ to be expressed as

$$\varrho^i(\theta) \approx \varrho^i(\theta_{ref}) \left(1 + \alpha^i(\theta)(\theta - \theta_{ref})\right)^{-3}. \tag{11}$$

The model of transformation induced plasticity (TRIP) applied only during the cooling process is based on Franitza-Mitter-Leblond proposal (cf. [2], [3], [9] and [16]). The corresponding equation for the case of multi-phase formations reads:

$$\begin{cases} \varepsilon^{\text{trip}}(t) &= 0, & t \le t_1 \\ \dot{\varepsilon}^{\text{trip}}(t) &= \dfrac{3}{2}\sigma^* \displaystyle\sum_{l=2}^{5} K_l^{\text{gj}}\left(\theta(t), z^l(\theta(t),t)\right) \left.\dfrac{d\phi_l(x)}{dx}\right|_{z_l(\theta(t),t)} \dot{z}^l(\theta(t),t), & t_1 \le t \le t_2 \end{cases} \tag{12}$$

where

$$\sigma^* = \sigma - \frac{1}{3}\text{tr}\sigma I \tag{13}$$

is the stress deviator, $K_l^{\text{gj}} \in C(\mathbb{R} \times [0,1])$ the respective Greenwood-Johnson parameter possibly depending on $\theta, z^l (l = 2, \cdots, 5), t$ and $\phi_l \in C[0,1] \cap C^1(0,1)$ the monotone saturation function with $\phi_l(0) = 0, \phi_l(1) = 1$. Here we assume volume conservation for the TRIP deformation, i.e.

$$\text{tr}(\varepsilon^{\text{trip}}) = 0. \tag{14}$$

According to (8) and to Hooke's law

$$\sigma = C\varepsilon^{\text{el}}, \tag{15}$$

with C being the elastic tensor we obtain

$$\sigma = C(\varepsilon(u) - \varepsilon^{\text{th}} - \varepsilon^{\text{trip}}). \tag{16}$$

For isotropic materials we introduce the commonly used Lamé coefficients λ, μ and the compression modulus $K = \lambda + \frac{2}{3}\mu$ to get the expressions of stress tensor for isotropic materials

$$\sigma = \lambda \,\text{div}\, uI + 2\mu\varepsilon(u) - 3K\varepsilon^{\text{th}} - 2\mu\varepsilon^{\text{trip}}. \tag{17}$$

Substituting (17) into (13), we obtain

$$\sigma^* = (\lambda - K)\text{div}uI + 2\mu\varepsilon(u) - 2\mu\varepsilon^{\text{trip}}.$$

In the equation of internal energy, Fourier's law gives

$$q = -k\nabla\theta, \tag{18}$$

with k the thermal conductivity.

To derive a constitutive relation for the internal energy e we introduce the Helmholtz-free energy Φ and the entropy s which are related by the thermodynamic identity

$$e = \Phi(\varepsilon^{\mathrm{el}}, \theta, z^1, \cdots, z^5) + \theta s. \tag{19}$$

With this definition, and following the ideas in [7, Section 2.3.2], we can obtain the thermo-mechanical equation for the heating process (without any TRIP effects) as

$$\varrho\dot{e} = \varrho c_\varepsilon \dot{\theta} + \sigma : \dot{\varepsilon}^{\mathrm{el}} + L_A \dot{z}^1, \tag{20}$$

and for the cooling process as

$$\varrho\dot{e} = \varrho c_\varepsilon \dot{\theta} + \sigma : \dot{\varepsilon}^{\mathrm{el}} - (L_F \dot{z}^2 + L_P \dot{z}^3 + L_B \dot{z}^4 + L_M \dot{z}^5), \tag{21}$$

where c_ε is the specific heat capacity and the constants L_A L_F, L_P, L_B, and L_M denote the latent heats of the Z^0-austenite, austenite-ferrite, austenite-pearlite, austenite-bainite, and austenite-martensite phase changes, respectively.

Inserting the above expressions (20) and (21) into (7), and using equations (8) and (18) we obtain the equations describing the heating process

$$\varrho c_\varepsilon \dot{\theta} - \mathrm{div}(k\nabla\theta) = -L_A \dot{z}^1 + \sigma : \dot{\varepsilon}^{\mathrm{th}} + h \tag{22}$$

and the cooling process

$$\varrho c_\varepsilon \dot{\theta} - \mathrm{div}(k\nabla\theta) = L_F \dot{z}^2 + L_P \dot{z}^3 + L_B \dot{z}^4 + L_M \dot{z}^5 + \sigma : (\dot{\varepsilon}^{\mathrm{th}} + \dot{\varepsilon}^{\mathrm{trip}}). \tag{23}$$

The mechanical dissipation is given by

$$\sigma : (\dot{\varepsilon}^{\mathrm{th}} + \dot{\varepsilon}^{\mathrm{trip}}) = \sigma : \dot{\varepsilon}^{\mathrm{th}} + \sigma : \dot{\varepsilon}^{\mathrm{trip}} \tag{24}$$

with (cf. (10))

$$\begin{aligned} &\sigma : \dot{\varepsilon}^{\mathrm{th}} \\ &= \left[\left(\sum_{i=0}^{5} z^i \alpha^i(\theta) + (\theta - \theta_{ref}) \sum_{i=0}^{5} z^i \alpha_\theta^i \right) \dot{\theta} + (\theta - \theta_{ref}) \sum_{i=0}^{5} \dot{z}^i \alpha^i(\theta) \right. \\ &\quad \left. - \frac{1}{3} \sum_{i=0}^{5} \dot{z}^i \left(\frac{\varrho^i(\theta_{ref})}{\varrho^0(\theta_{ref})} - 1 \right) \right] \times \mathrm{tr}\sigma \end{aligned} \tag{25}$$

where (cf.(10), (14), (17))

$$\mathrm{tr}\sigma = 3K \,\mathrm{div}\, u - 9K(\theta - \theta_{ref}) \sum_{i=0}^{5} z^i \alpha^i(\theta) + 3K \sum_{i=0}^{5} z^i \left(\frac{\varrho^i(\theta_{ref})}{\varrho^0(\theta_{ref})} - 1 \right) \quad (26)$$

and

$$\sigma : \dot{\varepsilon}^{\mathrm{trip}} = \frac{3}{2} |\sigma^*|^2 \sum_{l=2}^{5} K_l^{\mathrm{gj}}(\theta(t), z^l(\theta(t), t)) \frac{d\phi_l(x)}{dx}\bigg|_{z^l(\theta(t),t)} \dot{z}^l(\theta(t), t). \quad (27)$$

Based on (17) the thermomechanical equations (6) and (23) during cooling process can be reformulated as a coupled problem using a differential matrix operator A in the form

$$A \begin{pmatrix} u \\ \theta \end{pmatrix} = R(\theta, u, z, \dot{z}) \quad (28)$$

with

$$A := \begin{pmatrix} -\mu\triangle - (\lambda + \mu)\,\mathrm{grad}\,\mathrm{div} & 3K \,\mathrm{div} \sum_{i=0}^{5} z^i \alpha^i(\theta) P_I \\ f_1(\theta, z, \dot{z})\,\mathrm{div} & (\varrho c_\varepsilon + f_2(\theta, u, z, \dot{z}))\partial_t + f_3(\theta, u, z, \dot{z}) P_i - \nabla \cdot k \nabla \end{pmatrix}, \quad (29)$$

where the functions f_1, f_2 and f_3 are the remainders obtained from the above equations, the operators P_I, P_i are defined as

$$P_I(\theta) := \theta I, \quad (30)$$

$$P_i(\theta) := \theta, \quad (31)$$

and $R(\theta, u, z, \dot{z})$ is the corresponding right-hand side.

The main differences between the model presented here and the one in [7] is our approach for the TRIP modeling based on [3] and the decomposition of the thermal expansion in terms of density changes according to equation (10). This decomposition makes possible the implicit coupling between the temperature and the mechanical effects through thermal expanssion.

3. Simulations of the quenching process for the steel 42CrMo4

This section presents the simulation setting and some results of the quenching simulation applied to a gear component made of steel 42CrMo4. The model presented in Section 2 has been implemented on the toolbox pdelib [15] developed and maintained at WIAS-Berlin.

The simulation of the cogwheel has been performed making use of the inherent symmetries of the geometry constructed using the parameters as given in Table 1 and Figure 1. The simulation domain has been reduced from the complete piece to only one fourth of a tooth, which for the 21 teeth[1] means a total reduction of the simulation volume by a factor 84. The periodic geometry used for the simulations is shown in Figure 2.

Parameter		Value	
Module	m	2.00	[mm]
Pitchdiameter	d	42.00	[mm]
Outside diameter	D	47.75	[mm]
Pressure angle	$\hat{\theta}$	20.00	[°]
Face width	w	8.00	[mm]
Helix angle	ψ	0.00	[°]
Gear bore diameter	b	16	[mm]
Gear total surface	a	ca. 25.00	[cm^2]

Table 1: Characteristic values for the simulated cogwheel.

In order to perform a correct implementation of the component's geometry and properties, appropriate boundary conditions are required for the calculation of temperature, phases, and mechanical effects. The discrete system resulting from time and FEM discretization also includes the bi-directional coupling from temperature and mechanical deformation in the form presented in Section 2 (cf. equations (28)–(29)).

The next parts of this section are devoted to the description of the proper boundary conditions for the thermomechanical quenching problem, the mathematical weak formulation of the problem and its discretization, the material properties used for 42CrMo4, the initial values for the simulation and finally some numerical results on the evolution during the simulation.

[1]The number of teeth is defined as the ratio $N = d/m$.

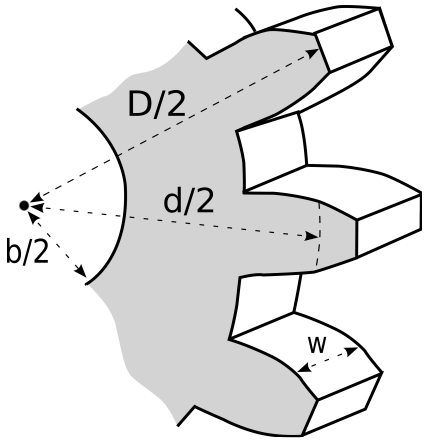

Figure 1: Definition of some parameters from Table 1.

3.1. Boundary conditions

In general, the thermal and mechanical boundary conditions of a domain Ω must be independently defined. For the mechanical boundaries, the boundary conditions might be set in terms of displacements, strains or stresses. The most common case is to define boundaries with predefined displacement or acting forces, i.e. split the mechanical boundaries into a part Γ_p where a pressure p is applied onto the surface of the boundary, and a part Γ_u where the deformation is fixed as $\hat{u}$ (including the case of fixed boundary). The mechanical boundary conditions on $\partial\Omega = \Gamma_p \cup \Gamma_u$ can be set as

$$\sigma_{ij}\nu_j = p, \text{ on } \partial\Gamma_p, \tag{32}$$

$$u = \hat{u}, \text{ on } \partial\Gamma_u. \tag{33}$$

For the case of the gear component we are interested in, the computations can be simplified by reducing the domain to a fourth of a tooth (cf. Figure 2). The reduction is obtained by considering the existent workpiece symmetries and using the corresponding constraints into the displacements' boundary conditions. The simulation geometry is obtained out of a single tooth from the 21 identical teeth. From this single cog, we consider only the fourth resulting from a radial cut from the middle of the tip towards the center of the gear, and another cut in traversal direction to the gear, slicing it at the half of its face width.

In this sense, outer faces in the computational domain do not necessarily represent outer faces in the real cogwheel geometry. The different nature

of the outer faces can be produced by considering a set of five different boundaries to form the complete boundary of Ω as $\Gamma = \Gamma_1 \cup \Gamma_2 \cup \Gamma_3 \cup \Gamma_4 \cup \Gamma_5$. The symmetry planes correspond to the planes $z = 0$ at Γ_5, $y = 0$ at Γ_4 and the oblique plane Γ_2.

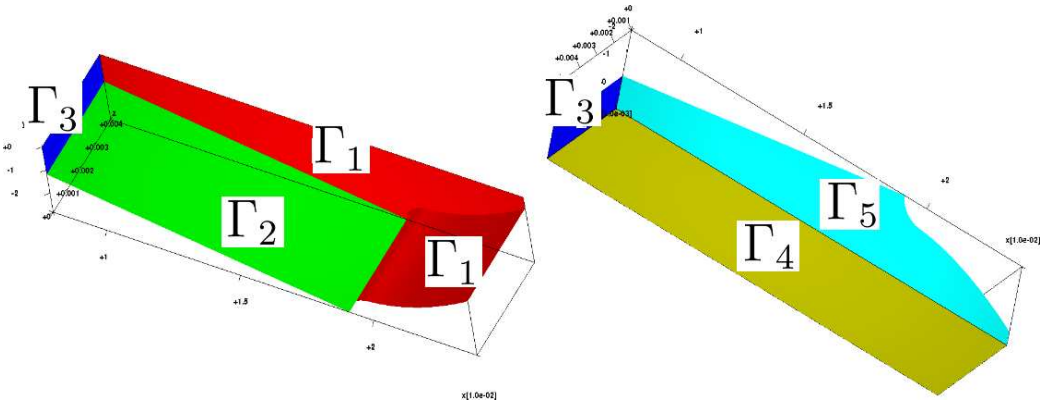

Figure 2: Computational domain Ω obtained as one fourth of a tooth.

According to Figure 2, the boundary Γ_1 corresponds to the real outer faces of the cogwheel and here we assume the boundary to be free of any acting force on them (p is zero according to the equation (32)). Another outer cogwheel boundary is Γ_3 and we assume the component as fixed from this side ($\hat{u} = (0, 0, 0)$ in equation (33)).

The other three boundaries correspond to inner parts of the real cogwheel geometry and must be included as symmetric cuts in the simulation domain.

For example, for the symmetry plane corresponding to the vertical cut at $z = 0$ (i.e. the boundary Γ_5), the z component of the displacement must equal zero. If we consider the existence of a neighboring domain $\tilde{\Omega}$ forming the symmetric counterpart of the domain Ω and sharing the boundary Γ_5, the deformation of the symmetric boundary must be equal to zero in the orthogonal direction to this boundary. A similar idea supports the statement that the changes (space derivatives) in the components x and y of the deformation u must be also zero, as any positive (negative) value would mean a negative (positive) value in the symmetric domain, causing the strain and stress tensors to have singularities in form of jumps at the symmetry plane Γ_5. These two ideas for Γ_5 can be written in the form $u^z = 0$, $\nabla u^x \cdot \vec{n}_5 = 0$ and $\nabla u^y \cdot \vec{n}_5 = 0$, where the superscripts on the deformation variable represent its three components, i.e. $u = (u^x, u^y, u^z)$ and $\vec{n}_5$ the normal to the

surface Γ_5.

Following similar ideas for the symmetry planes Γ_2 and Γ_4, the complete set of boundary conditions for the balance law of momentum (6) read

$$\begin{cases} \sigma \cdot \vec{n}_1 = 0, & \text{on } \Gamma_1 \\ u \cdot \vec{n}_2 = 0, & \text{on } \Gamma_2 \\ \nabla u^z \cdot \vec{n}_2 = 0, & \text{on } \Gamma_2 \\ \nabla (u \cdot \vec{n}_2^{\perp}) \cdot \vec{n}_2 = 0, & \text{on } \Gamma_2 \\ u = 0, & \text{on } \Gamma_3 \\ u \cdot \vec{n}_4 = 0, & \text{on } \Gamma_4 \\ \nabla u^x \cdot \vec{n}_4 = 0, & \text{on } \Gamma_4 \\ \nabla u^z \cdot \vec{n}_4 = 0, & \text{on } \Gamma_4 \\ u \cdot \vec{n}_5 = 0, & \text{on } \Gamma_5 \\ \nabla u^x \cdot \vec{n}_5 = 0, & \text{on } \Gamma_5 \\ \nabla u^y \cdot \vec{n}_5 = 0, & \text{on } \Gamma_5 \end{cases} \tag{34}$$

where each vector $\vec{n}_i$ represents the normal to the surface Γ_i and $\vec{n}_2^{\perp}$ is the direction on the surface Γ_2 which is orthogonal to both $\vec{n}_2$ and the z-direction. Particularly according to our selected Cartesian coordinate system we obtain the vectors

$$\begin{array}{llll} \vec{n}_4 & = (0 \quad 1 \quad 0)^T, & \vec{n}_5 & = (0 \quad 0 \quad -1)^T, \\ \vec{n}_2 & = (n_2^x \quad n_2^y \quad 0)^T, & \vec{n}_2^{\perp} & = (n_s^x \quad n_s^y \quad 0)^T \end{array} \tag{35}$$

with $n_2^x n_s^x + n_2^y n_s^y = 0$. The values of the components n_2^x and n_2^y can be easily obtained by using the value of the plane-to-plane angle between Γ_2 and Γ_4 which is equal to

$$\phi = \frac{1}{2} \cdot \frac{360^\circ}{d/m} \approx 8.5714^\circ. \tag{36}$$

The boundary conditions for the heat equation are much simpler, as the temperature is a scalar unknown and there are only two types of boundaries: the ones which have a thermal flow during quenching and the ones considered as symmetry planes at which the thermal flow must be assumed to be zero. The heat equation (23) has then the boundary conditions

$$\begin{cases} -k \nabla \theta \cdot \vec{n}_1 = \delta(\theta - \theta_{ext}), & \text{on } \Gamma_1 \\ -k \nabla \theta \cdot \vec{n}_i = 0, & \text{on } \Gamma_i (i = 2, \cdots, 5) \end{cases} \tag{37}$$

where θ_{ext} is the temperature of the cooling solution being sprayed at the component to quench it.

3.2. Weak formulation and Discretization

Having in mind all previous boundary conditions we introduce the weak formulation of the problems (6) and (23):

Find $\theta(t) \in H^1(\Omega)$ and $u(t) \in X^u$ with

$$X^u := \{\varphi \in (H^1(\Omega))^3; \quad \varphi \cdot \vec{n}_2|_{\Gamma_2} = 0,\ \varphi \cdot \vec{n}_4|_{\Gamma_4} = 0,\ \varphi \cdot \vec{n}_5|_{\Gamma_5} = 0,\ \varphi|_{\Gamma_3} = 0\} \tag{38}$$

such that

$$\begin{aligned} \int_\Omega \sigma \cdot \nabla\varphi dx &= 0, \\ \int_\Omega \varrho c_\varepsilon \dot{\theta}\psi dx + \int_\Omega k\nabla\theta \cdot \nabla\psi dx &= \int_\Omega (L_F\dot{z}^2 + L_P\dot{z}^3 + L_B\dot{z}^4 + L_M\dot{z}^5)\psi dx \\ &\quad + \int_\Omega (\sigma : (\dot{\varepsilon}^{\mathrm{th}} + \dot{\varepsilon}^{\mathrm{trip}}) + h)\psi dx \end{aligned} \tag{39}$$

for all $\varphi \in X^u, \psi \in H^1(\Omega)$ and a.e. $t \in [t_1, t_2)$.

Remark. Based on the boundary conditions (34) and the formula for integration by parts, it is easy to verify that

$$\int_\Omega -(\operatorname{div}\sigma) \cdot \varphi dx = \int_\Omega \sigma : \varepsilon(\varphi) = 0 \tag{40}$$

due to the absence of any stresses in orthogonal direction at any domain boundary.

Allowing for variable time-step sizes let $M_1, M_2 \in \mathbb{N}$ be fixed, $t_0 = t^0 < t^1 < \cdots < t^{M_1} = t_1 < t^{M_1+1} < \cdots t^{M_2} = t_2$ be a partition of interval $[t_0, t_2]$ and $\triangle t^m = t^m - t^{m-1}$. Since we consider here the cooling process let $M_1 < m \leq M_2$. Define z_m^i $(i = 0, \cdots, 5)$ as an approximation of the phases' volume fraction at time t^m. The phases z_m^i can be calculated as the discrete solutions of the ODE-system in (5) (this can be performed by e.g. an explicit-Euler method on then system). Similarly, let $u_m := u(t^m)$ and $\theta_m := \theta(t^m)$.

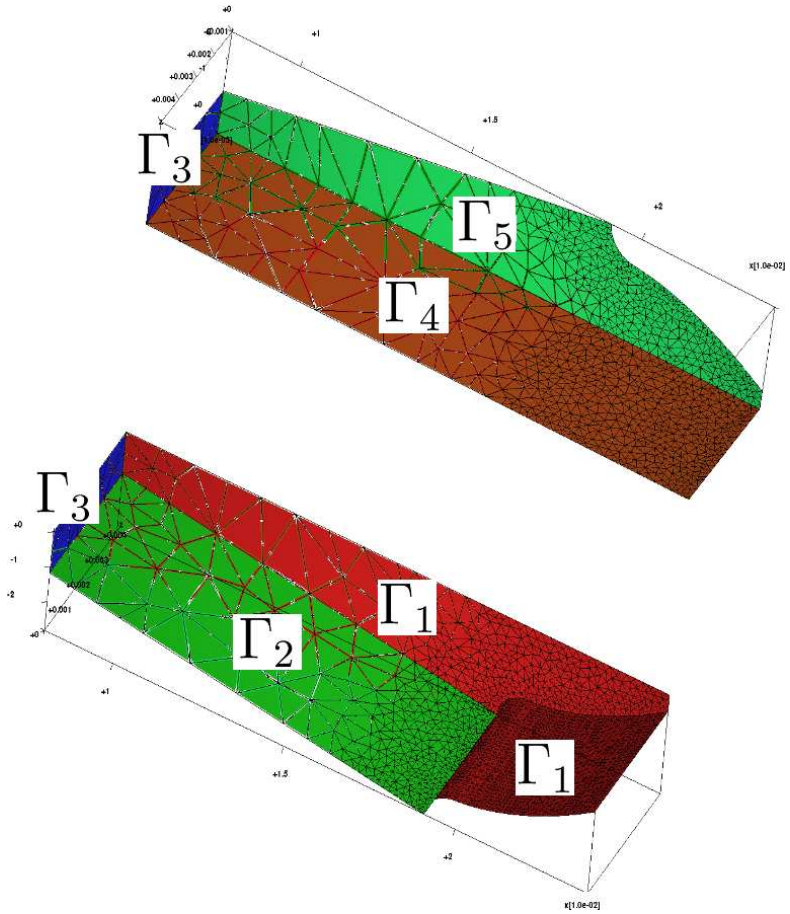

Figure 3: Two different views of the domain discretization using tetrahedral elements. The different boundaries are labeled according to the equations in (34).

For the spatial discretization of the PDEs we apply the Finite Element method. We choose a conforming triangulation of Ω (cf. Figure 3) and then use piecewise polynomial Lagrange Finite Elements ϕ for the definition of the corresponding FE-space X_h^u according to X^u.

More precisely, let N_{Γ_1}, N_{Γ_2}, N_{Γ_4}, N_{Γ_5}, N_Ω, $N_{\Omega/\Gamma}$ denote sets of numbers which indicate degrees of freedom (in linear case also the vertices) of Γ_1, Γ_2, Γ_4, Γ_5, all degrees of freedom, and the interior discrete points of Ω, respectively. Then we can write the discrete space X_h^u as the direct sum of the five subspaces for the sets of degrees of freedom as

$$X_h^u := U_1 \oplus U_2 \oplus U_4 \oplus U_5 \oplus U_{in} \tag{41}$$

where

$$U_1 := \operatorname{span}\left\{ \begin{pmatrix}\phi_i\\0\\0\end{pmatrix}, \begin{pmatrix}0\\\phi_i\\0\end{pmatrix}, \begin{pmatrix}0\\0\\\phi_i\end{pmatrix} \right\}_{i\in N_{\Gamma_1}}, \tag{42}$$

$$U_2 := \operatorname{span}\left\{ \begin{pmatrix}\frac{n_s^x}{n_s^y}\phi_l\\\phi_l\\0\end{pmatrix}, \begin{pmatrix}0\\0\\\phi_l\end{pmatrix} \right\}_{l\in N_{\Gamma_2}}, \tag{43}$$

$$U_4 := \operatorname{span}\left\{ \begin{pmatrix}\phi_j\\0\\0\end{pmatrix}, \begin{pmatrix}0\\0\\\phi_j\end{pmatrix} \right\}_{j\in N_{\Gamma_4}}, \tag{44}$$

$$U_5 := \operatorname{span}\left\{ \begin{pmatrix}\phi_k\\0\\0\end{pmatrix}, \begin{pmatrix}0\\\phi_k\\0\end{pmatrix} \right\}_{k\in N_{\Gamma_5}}, \tag{45}$$

$$U_{in} := \operatorname{span}\left\{ \begin{pmatrix}\phi_s\\0\\0\end{pmatrix}, \begin{pmatrix}0\\\phi_s\\0\end{pmatrix}, \begin{pmatrix}0\\0\\\phi_s\end{pmatrix} \right\}_{s\in N_{\Omega/\Gamma}}. \tag{46}$$

The exact solutions θ_m, u_m will be approximated as linear combinations of the basis of $V_h := \operatorname{span}\{\phi_i\}_{i\in N_\Omega} \subset H^1(\Omega)$ and X_h^u respectively, more precisely,

$$\theta_m \approx \sum_{i\in N_\Omega} T_m^i \phi_i, \tag{47}$$

$$u_m \approx \sum_{i\in N_\Omega} \left(U_m^{1,i} \begin{pmatrix}\phi_i\\0\\0\end{pmatrix} + U_m^{2,i} \begin{pmatrix}0\\\phi_i\\0\end{pmatrix} + U_m^{3,i} \begin{pmatrix}0\\0\\\phi_i\end{pmatrix} \right) \tag{48}$$

where

$$U_m^{1,i} = 0 \qquad \text{for all} \quad i \in N_{\Gamma_3}, \tag{49}$$

$$U_m^{2,i} = 0 \qquad \text{for all} \quad i \in N_{\Gamma_3} \cup N_{\Gamma_4}, \tag{50}$$

$$U_m^{3,i} = 0 \qquad \text{for all} \quad i \in N_{\Gamma_3} \cup N_{\Gamma_5}, \tag{51}$$

$$n_s^1 U_m^{2,i} = n_s^2 U_m^{1,i} \qquad \text{for all} \quad i \in N_{\Gamma_2}. \tag{52}$$

In order to get a numerical solution, we introduce the time-discrete version of the system (28)–(29) as

$$A_{m-1} \begin{pmatrix}u_m\\\theta_m\end{pmatrix} = R_{m-1}, \tag{53}$$

where

$$A_{m-1} = \begin{pmatrix} -\mu\triangle - (\lambda+\mu)\,\mathrm{grad}\,\mathrm{div} & 3K\,\mathrm{div}\sum_{i=0}^{5} z_{m-1}^{i}\alpha^{i}(\theta_{m-1})P_I \\ f_{1_{m-1}}\,\mathrm{div} & (\varrho_{m-1}c_{\varepsilon_{m-1}} + f_{2_{m-1}})\dfrac{1}{\triangle t^m} + f_{3_{m-1}}P_i - \nabla\cdot k_{m-1}\nabla \end{pmatrix}. \tag{54}$$

the right hand side is

$$R_{m-1} = R\left(\theta_{m-1}, u_{m-1}, z_m, \frac{z_m - z_{m-1}}{\Delta t^m}\right) + \begin{pmatrix} 0 \\ (\varrho_{m-1}c_{\varepsilon_{m-1}} + f_{2_{m-1}})\dfrac{1}{\Delta t^m}\theta_{m+1} \end{pmatrix}, \tag{55}$$

and the phase fractions correspond to the previously computed values using the temperature evolution up to the previous time step.

Let $\mathbf{T}_m, \mathbf{U}_m$ be the corresponding coefficient vectors of (47)–(48), then applying Galerkin's method to the time discrete system (53)–(55) we can assemble the global matrix $\mathbf{A}_{m-1}$ using boundary conditions (34), (37) and (49)–(52) to obtain a set of linear equations

$$\mathbf{A}_{m-1}\begin{pmatrix}\mathbf{U}_m \\ \mathbf{T}_m\end{pmatrix} = \mathbf{R}_{m-1}. \tag{56}$$

The solution of the equations for the phase fractions as well as the coupled system of equations (56) give the values of the discretized temperature and the deformation at the time t^m. This is done for all time steps in the complete time interval $[t_1, t_2]$.

3.3. Material parameters for 42CrMo4

The numerical simulations using the geometry in Figure 3 are carried out on a cogwheel made of steel 42CrMo4, which has a chemical composition according to Table 2.

C	Si	Mn	P	S	Cr	Ni	Mo	Sn	Al
0.431	0.301	0.707	0.019	0.13	1.003	0.098	0.197	0.013	0.021

Table 2: Chemical composition of the steel 42CrMo4 (taken from [11]).

All material parameters throughout this paper have been provided by the IWT (Stiftung Institut für Werkstoffstechnik Bremen, Germany) and some

of them are taken from the reference [11] if not specified otherwise. The following list presents all used parameters as implemented in the numerical simulation:

- Reference temperature: $\theta_{ref} = 20°\mathrm{C}$
- External temperature: $\theta_{ext} = 20°\mathrm{C}$
- Reference density, [kg/m^3]:

ϱ^0_{ref}	ϱ^1_{ref}	ϱ^2_{ref}	ϱ^3_{ref}	ϱ^4_{ref}	ϱ^5_{ref}
7820.7	8037	7825	7825	7782	7783

  The reference density of the initial phases' mixture z_0 has been obtained by assuming a composition of the material with 90% ferrite-pearlite and 10% bainite volume fractions. These fractions are used as weights to obtain $\varrho^0_{ref} = \sum_{i=1}^{5} \varrho^i_{ref}$. The resulting mixed density coincides with the measured density for our steel 42CrMo4.

- Thermal expansion coefficient [$10^{-6}\,\mathrm{K}^{-1}$]:

$\alpha^0(\theta)$	$\alpha^1(\theta)$	$\alpha^2(\theta)$	$\alpha^3(\theta)$	$\alpha^4(\theta)$	$\alpha^5(\theta)$
14.5	23.3	14.5	14.5	14.5	14.5

- Specific heat capacity $c_\varepsilon(\theta)$ [J/kg K]:

  This material constant has been approximated to experimental data by one cubic polynomial for low temperatures, a linear polynomial for high temperatures, and a series of linear interpolations for the intermediate temperatures as

$$c_\varepsilon(\theta) = \begin{cases} a\tilde{\theta}^3 + b\tilde{\theta}^2 + c\tilde{\theta} + d & \text{for } \theta \leq 706.8°\mathrm{C}, \\ \mathcal{I}(\tilde{\theta}) & \text{for } 706.8°\mathrm{C} < \theta < 786.8°\mathrm{C}, \\ e\tilde{\theta} + f & \text{for } \theta \geq 786.8°\mathrm{C}, \end{cases}$$

  where $\tilde{\theta}$ represents the non-dimensional temperature $\tilde{\theta} = \theta/°\mathrm{C}$. The polynomial coefficients are given as

Parameter	Value	[J/Kg K]
a	1.10	E-8
b	3.45	E-4
c	4.94	E-1
d	4.00	E+2
e	1.55	E-1
f	4.73	E+2

and $\mathcal{I}$ represents the linear interpolation operator for the intermediate temperatures with the points

$\tilde{\theta}$	706.8	786.8
c_ε [J/kg K]	973	595

- Heat conductivity, [W/m K]

$$k(\theta, z) = \begin{cases} \left(-0.000024\tilde{\theta}^2 - 0.000978\tilde{\theta} + 43.275917\right) \frac{\mathrm{W}}{\mathrm{m\,K}} & \text{for } \theta < 810°C, \\ \left(0.008148\tilde{\theta} + 20.211620\right) \frac{\mathrm{W}}{\mathrm{m\,K}} & \text{for } 810°\mathrm{C} \leq \theta. \end{cases}$$

- Lamé coefficients [kg/m s^2]:

  $\lambda = 1.07 \times 10^{11}, \qquad \mu = 6.88 \times 10^{10}$

- Heat transfer coefficient: $\delta = 12 \times 10^3 \quad \frac{\mathrm{W}}{\mathrm{m^2K}}$

- Parameters for the phase transitions according to equations (1) and (5), mainly taken from [11].

  Critical temperatures for the activation of phase transformations

F_{P_s}	F_{P_f}	B_s	B_f	M_s	M_f
750°C	580°C	600°C	140°C	340°C	140°C

  Parameter $b(\theta) = 10^{c+c_1\theta+c_2\theta^2+c_3\theta^3}$ where

c	c_1	c_2	c_3
-309.075	1.45	-0.00227	0.000001175

  Parameter $a(\theta) = d + d_1\theta + d_2\theta^2 + d_3\theta^3$ where

d	d_1	d_2	d_3
37.44	-0.238	0.000474	-0.000000295

Parameter $\tilde{b}(\theta) = 10^{\tilde{c}+\tilde{c}_1\theta+\tilde{c}_2\theta^2+\tilde{c}_3\theta^3}$ where

$\tilde{c}$	$\tilde{c}_1$	$\tilde{c}_2$	$\tilde{c}_3$
-7.763	0.0168	0.000001078	-0.0000000253

Parameter $\tilde{a}(\theta) = \tilde{d} + \tilde{d}_1\theta + \tilde{d}_2\theta^2 + \tilde{d}_3\theta^3$ where

$\tilde{d}$	$\tilde{d}_1$	$\tilde{d}_2$	$\tilde{d}_3$
41.365	-0.222	0.000398	-0.000000232

Parameter $n = 2.5$

- Latent heat [MJ/m^3]:

L_A	L_F	L_P	L_B	L_M
652	652	652	652	326

- TRIP parameters according to equation (12):

  Greenwood-Johnson Parameter

  $K_l^{gj} = 5.2 \cdot 10^{-11}$ Pa^{-1} $(l = 2, \cdots, 5)$.

  Saturation function: Identity function.

3.4. Initial values

The initial values $z^1(t_1), u(t_1), \theta(t_1)$ to use in the simulation of the cooling process need to be obtained experimentally or through a simulation of the heating process. The latter can be performed by solving the coupled system of equations (5), (6), and (22) with an appropriate external heat source h. In the case of induction hardening, this thermal source consists of the contribution of the Joule heat.

Since we consider here only the simulation of the quenching process, we use initial values for $z^1(t_1)$ and $\theta(t_1)$ taken from a heating simulation calibrated for the inductive heating of the same component[2].

Figure 4 shows the values of temperature on the three-dimensional simulation domain (cf. Figures 2 and 3). The temperature corresponds to the final stage after inductive heat with high frequency has been introduced into the workpiece. The shown deformation is an effect of thermal expansion

[2]The simulations presented here make use of the heating results provided by our cooperation partner WIAS. The provided data include the component temperature and austenite profile.

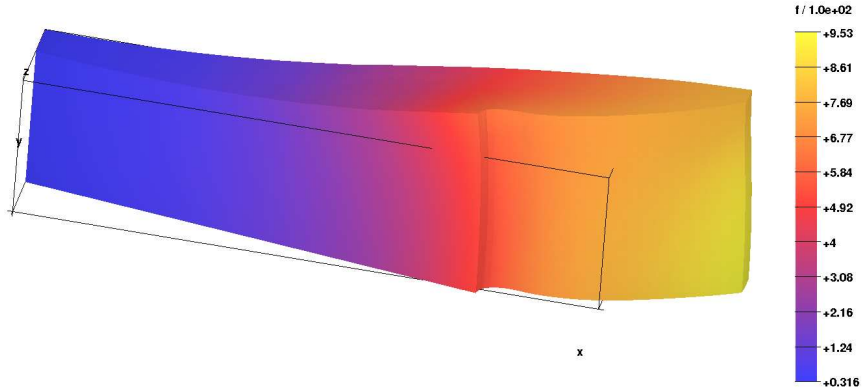

Figure 4: Initial temperature $\theta(t_1)$ plotted on the deformed geometry. The deformation (scaled by a factor of 40) results from the thermal expansion due to temperature increase.

through temperature change with respect to the reference temperature. The deformation in the piece has been scaled by a factor of 40 to improve its visualization.

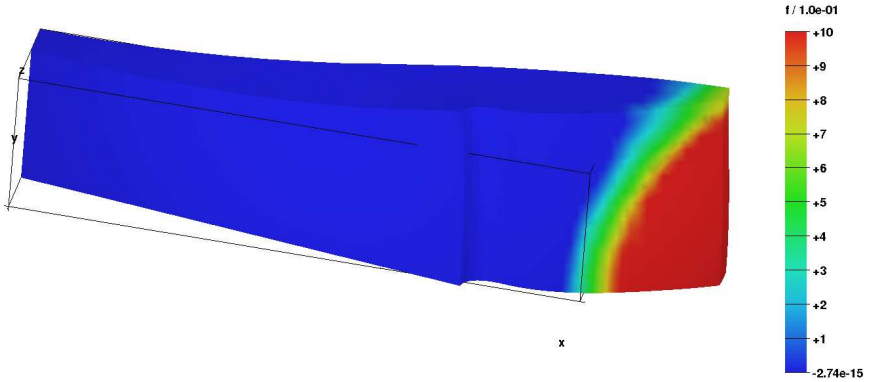

Figure 5: Initial austenite phase fraction $z^1(t_1)$ plotted on the deformed geometry.

Figure 5 shows the initial state of austenite, being transformed from z^0 during the prior heating process. The red colored area represents the volume formed by 100% austenite and its shape depends on the parameters during the inductive heating. Given the temperature and initial state of the different phases, the equations (6) and (12) can be solved to obtain the corresponding deformation, strain, and stress. Figure 6 shows the deformed geometry and the norm of the deformation (color scale). The deformation has its largest

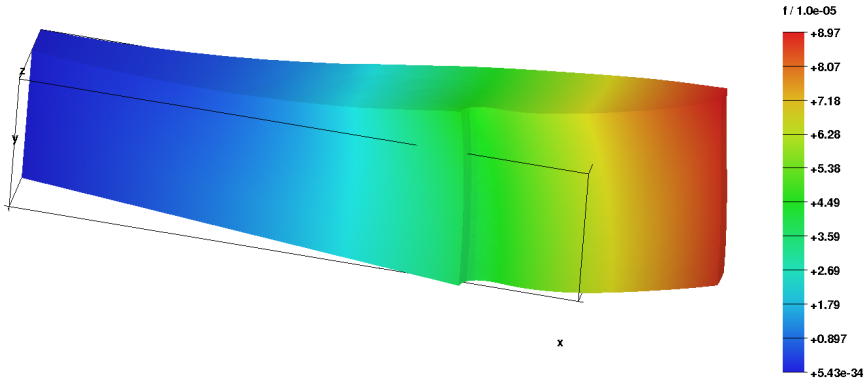

Figure 6: Computed norm of the initial deformation $||u(t_1)||_{L^2(\Omega)}$.

values in the area where the temperature has the largest values as a direct effect of the thermal expansion.

3.5. Numerical results

The simulation based on the material data and initial values from Sections 3.3 and 3.4 computes the discrete solutions using the system in equation (56). Table 3 shows the computational expenses to get the results presented below, using the tetrahedral discretization of the geometry as displayed in Figure 3.

Processor:	Intel Core i7-2600, 3.4 GHz
Installed RAM:	16.0GB
Total computation time:	ca. 26 h
Mesh nodes:	6514
Tetrahedral elements	32246
Number of time steps:	11000

Table 3: Computational expenses.

For the quenching simulation, it is clear that the temperature should decrease, producing changes also in the deformation and the phases. Figure 7 shows the progressive temperature values on the side view of the deformed geometries for five different simulated times. In the plots from Figure 7 it can be observed how the very hot areas cool down in less than one second, getting homogeneous values close to the reference temperature for an elapsed time of 2.4 seconds.

The contraction of the component can also be observed in these plots. The strong deformation on the outer areas of the cogwheel disappears and leaves some deformed areas close to the outer corners of the component. Although at the beginning the workpiece geometry has a rather homogeneous expanded volume at the tooth tip due to the high temperature, the final shape presents some more localized distortion effects, created by the change in densities due to phase transformations and the inelastic TRIP effects.

From the practitioner's point of view, the most important transformation is the change from austenite into martensite, as the martensitic content will determine the hardness of the component after the heat treatment process is finished.

This developement is presented in Figure 8, where the evolutions of both phase fractions are presented in parallel. In these plots, it can be observed

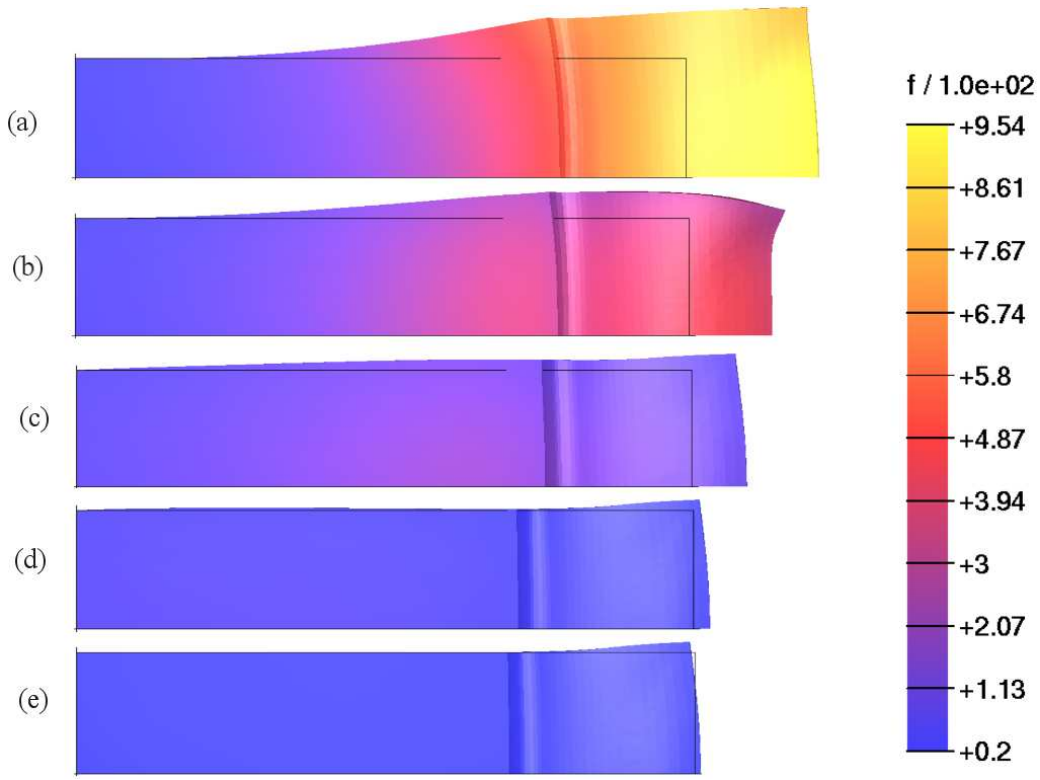

Figure 7: Temperature evolution for five different simulation times: (a) $t = 0$ (initial state), (b) $t = 0.24s$, (c) $t = 0.84s$, (d) $t = 2.4s$, (e) $t = 11s$.

how the austenite content gradually disappears, first in the areas close to the component corners (these are also the areas with the fastest heat outflow) and later in the not so close areas. The opposite occurs with the martensitic phase, being inexistent at the beginning and becoming the dominant phase in the areas close to the corners of the component. Note that all the times shown in Figure 8 correspond to the first second of the quenching process. After this time nothing else is changed, as the minimal activation temperature of martensite has already been reached (cf. equation (5)).

The final deformation of the domain corresponds to the typical volume growth in areas where the austenite phase is transformed into martensite, changing the density to a lower value (cf. material parameters in Section 3.3) and producing the increment in volume.

Much less important is the evolution of ferrite, pearlite and bainite, as they do not appear in such a fast cooling process. The results in Figure 9 confirm this, showing the final states for these phase fractions. They are all far from reaching any significant amount, so that they can be considered as non

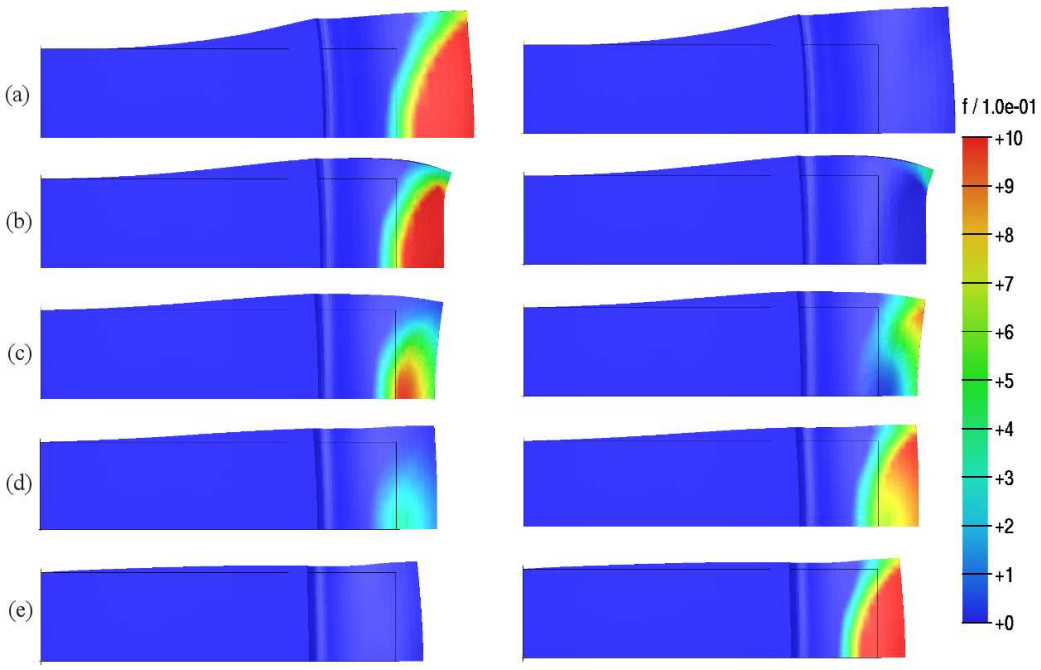

Figure 8: Comparison of austenite and martensite evolutions at different simulation times: (a) $t = 0$ (initial state), (b) $t = 0.24s$, (c) $t = 0.38s$, (d) $t = 0.5s$, (e) $t = 0.98s$.

existent. Their evolution might become important for different temperature evolutions and we present them here only for completeness.

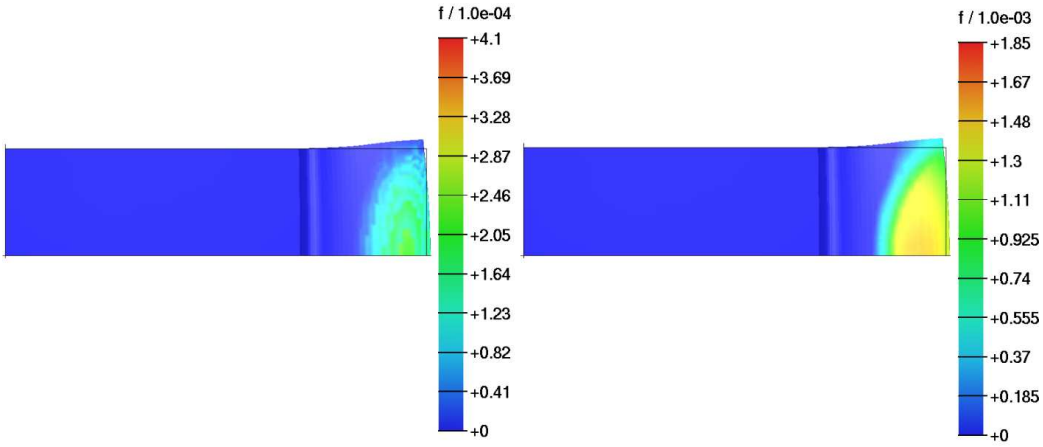

Figure 9: Volume fraction of ferrite+pearlite (left) and bainite (right) at simulation time $t = 11s$ (end state). The maximal volume fracion of ferrite+pearlite is 0.041% and of bainite 0.185%.

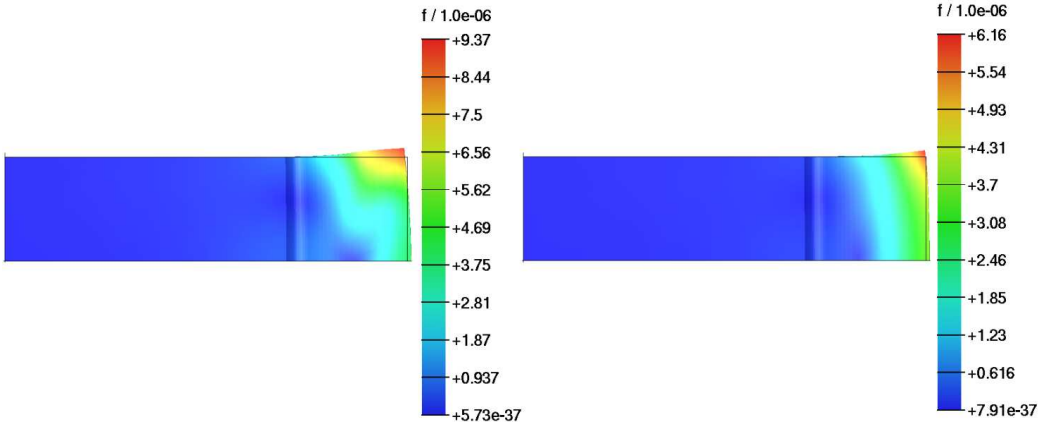

Figure 10: Norm of displacement at $t = 11s$ (end state) for the simulation including TRIP simulation (left) and the simulation without it (right).

One important issue during the implementation of the simulation was whether the TRIP effect significantly influences the results or not. For this reason, the simulation was carried out two times, with and without considering this part of the model.

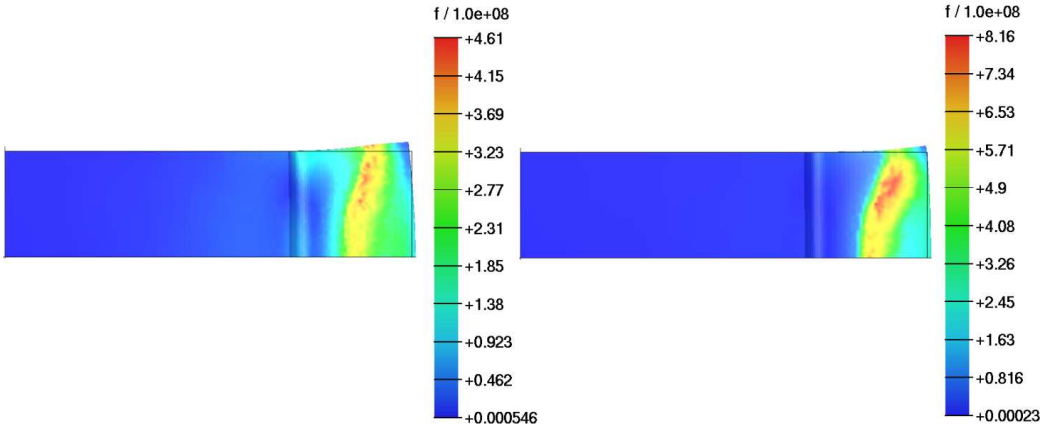

Figure 11: Equivalent (von Mises) stress at $t = 11s$ (end state) for the simulation including TRIP simulation (left) and the simulation without it (right).

The results of deformation and stress are shown in Figures 10 and 11. It is obvious that both the final deformation and the stress present different results in the simulations. Regarding the von Mises stress, the model with TRIP seems to have a smaller area affected by large stresses. The stress distributions at the end of the simulations are also quantitatively different, giving maximum values of 461 MPa and 816 MPa for the models with and without TRIP, respectively. Note that the stress value for the model without TRIP can be by far over the yield stress for the 42CrMo4 steel, with values around the 600 MPa.

4. Conclusions

A thermomechanical model for induction surface hardening including occurring phase transitions that produce the hardening effect has been investigated. In the simulations of cooling process presented here, owing to high cooling rates most of the austenite is transformed to martensite and the formations of ferrit, perlit and bainite are negligible (always less than 0.2%). Concerning the effect of TRIP, a comparison has shown that the consideration of TRIP produces significant differences in the results and therefore cannot be neglected.

Although the differences in the models with and without TRIP produce different results, it is still not clear if the TRIP is the only inelastic term to be considered, as also the use of a model for classical plasticity might be of

interest.

Since only the cooling process has been simulated, the consideration of efficient solvers for the heating process, i.e. coupled problem of Maxwell's equation, heat equation and deformation behavior under consideration of phase transformations is an important direction of further research. An option would be to obtain a heat source from the electromagnetic simulation and then use it for a complete thermomechanical simulation where the heating and quenching processes will be computed together. The simulation of the heating process would also allow the consideration of inelastic effects appearing during the temperature increase, either through phase changes or classical plasticity effects.

Acknowledgements

The authors gratefully acknowledge the financial support of the "Bundesministerium für Bildung und Forschung" (BMBF) within the project "Modellierung, Simulation und Optimierung des Mehrfrequenzverfahrens für die Induktive Wärmebehandlung (MeFreSim)" at the University of Bremen. Special thanks go to our cooperation partners within the MeFreSim research network for providing the material properties and initial data for the simulation.

Symbols

θ	temperature
θ_{ref}	reference temperature
θ_{ext}	external temperature
ϱ^i_{ref}	density of $z^i (i = 0, \ldots, 5)$ at θ_{ref}
$\varrho(\theta, z)$	density
$c_\varepsilon(\theta, z)$	specific heat
$k(\theta, z)$	heat conductivity
q	heat flux
h	heat source
$\delta(\theta, z)$	heat transfer coefficient
u	displacement
$\varepsilon(u) = \frac{1}{2}(\nabla u + \nabla u^T)$	strain tensor
$\varepsilon^{\mathrm{el}}$	elastic strain
$\varepsilon^{\mathrm{th}}$	thermal strain

$\varepsilon^{\text{trip}}$	TRIP strain
σ	stress tensor
$\alpha^i(\theta)$	thermal expansion coefficient of phase z^i
λ, μ	Lamé coefficients
$K = \lambda + \frac{2}{3}\mu$	bulk modulus
$z = (z^0, z^1, \ldots, z^5)^T$	vector of phases
L_A	z^0–austenite latent heat
L_F	austenite–ferrite latent heat
L_P	austenite–pearlite latent heat
L_B	austenite–bainite latent heat
L_M	austenite–martensite latent heat
F_{Ps}	ferrite and pearlite start temperature
F_{Pf}	ferrite and pearlite end temperature
B_s	bainite start temperature
B_f	bainite end temperature
M_s	martensite start temperature
M_f	martensite end temperature
K_l^{gj}	Greenwood-Johnson parameter

References

[1] N. Bontcheva, G. Petzov: *Total simulation model of the thermo-mechanical process in shape rolling of steel rods.* Comp. Mater. Sci., 34, No. 1, (2009) 377-388.

[2] F.D. Fischer, Q.P. Sun, K. Tanaka: *Transformation-Induced Plasticity (TRIP).* Appl. Mech. Rev., Vol 49, (1996), p 317-364

[3] F.D. Fischer, G.Reisner, E. Werner, K. Tanaka, G.Cailletaud, T. Antretter: *A new view on transformation induced plasticity (TRIP).* International Journal of Plasticity 16 (2000), 723-748.

[4] D. Hömberg: *A mathematical model for the phase transitions in eutectoid carbon steel.* IMA Journal of Applied Mathematics 54 (1995), 31-57.

[5] D. Hömberg: *A numerical simulation of the Jominy end-quench test.* Acta Mater., 44 (1996), 4375-4385.

[6] D. Hömberg: *Irreversible phase transitions in steel.* Math. Methods Appl. Sci., 20 (1997), 59-77.

[7] D. Hömberg: *A mathematical model for induction hardening including mechanical effects.* Nonlinear Anal. Real World Appl. 5 (2004), 55-90.

[8] J.-B. Leblond, J. Devaux: *A new kinetic model for anisothermal metallurgical transformations in steels including effect of austenite grain size.* Acta Met. 32, (1984), 137-146.

[9] J.-B. Leblond, J. Devaux, J.C. Devaux: *Mathematical Modelling of Transformation Plasticity in Steels. I: Case of Ideal-Plastic Phases.* Int. J. Plast., Vol 5, (1989), p 551-572

[10] J. Lemaitre, J.-L. Chaboche: *Mechanics of Solid Materials.* Cambridge University Press, Cambridge, 1990.

[11] T. Mioković: *Analyse des Umwandlungsverhaltens bei ein- und mehrfacher Kurzzeithärtung bzw. Laserstrahlhärtung des Stahls 42CrMo4.* Dissertation, Shaker Verlag Aachen 2005.

[12] J. Montalvo-Urquizo, Z. Akbay, A. Schmidt: *Adaptive finite element models applied to the laser welding problem.* Comp. Mater. Sci., 46 No. 1, (2009) 245-254.

[13] R. Schröder: *Untersuchung zur Spannungs- und Eigenspannungsausbildung beim Abschrecken von Stahlzylindern.* Dissertation, Universität Karlsruhe, 1985.

[14] C. Şimşir, C. H. Gr: *A FEM based framework for simulation of thermal treatments: Application to steel quenching.* Comp. Mater. Sci. 44 No. 2, (2008) 588-600.

[15] T. Streckenbach, J. Fuhrmann, H. Langmach, M. Uhle: *Pdelib– A software toolbox for numerical computations* http://www.wias-berlin.de/software/pdelib/ (2010) Retrieved 31.1.2013.

[16] L. Taleb, F. Sidoroff: *A Micromechanical Modeling of the Greenwood-Johnson Mechanism in Transformation-Induced Plasticity.* Int. J. Plast., 19, (2003), 1821-1842

[17] C. Verdi, A. Visintin: *A mathematical model of the austenite-pearlite transformation in plain steel based on the Scheil's additivity rule.* Acta Metall., 35, No. 11 (1987), 2711-2717.

[18] A. Visintin: *Mathematical models of solid-solid phase transitions in steel.* IMA J. Appl. Math., 39 (1987), 143-157.

[19] M. Wolff, M. Böhm, S. Böttcher: *Phase transformations in steel in the multi-phase case - gerneral modelling and parameter identification.* Technical Report 07-02, Universität Bremen, Berichte aus der Technomathematik, 2007.